Electronic Supplementary Information

Optical Properties of Organometal Halide Perovskite Thin Films and General Device Structure Design Rules for Perovskite Single and Tandem Solar Cells

Chang-Wen Chen, [a] Sheng-Yi Hsiao, [a] Chien-Yu Chen, [a] Hao-Wei Kang, [a] Zheng-Yu Huang [a] and Hao-Wu Lin* [a]

[a] Department of Materials Science and Engineering, National Tsing Hua University, No. 101, Section 2, Kuang-Fu Road, Hsinchu, Taiwan 30013.
E-mail: hwlin@mx.nthu.edu.tw

Experimental Methods

Perovskite thin-film preparation: The PEDOT:PSS (*Clevios AI 4083*) thin film was prepared on pre-cleaned ITO substrates by spin coating. The PEDOT:PSS-coated substrates were then loaded into a high vacuum chamber (base pressure $< 1 \times 10^{-6}$ torr) to evaporate $PbCl_2$ and CH_3NH_3I thin films layer-by-layer. The $PbCl_2$ layers were thermally sublimed onto PEDOT:PSS-coated ITO glass with a constant deposition rate of 1.5 Å/s. During the $PbCl_2$ deposition procedure, the substrates were kept at room temperature. CH_3NH_3I was then sublimed onto the $PbCl_2$ layers with a constant source temperature of 85 °C. The substrates were controlled at 75 °C during deposition of the CH_3NH_3I layers. Upon deposition of CH_3NH_3I, $PbCl_2$ reacted with CH_3NH_3I *in situ* and formed flat perovskite thin films ($CH_3NH_3PbI_{3-x}Cl_x$). A post-annealing process at 100 °C was applied for a short period (several minutes) to fully crystallise the perovskite film. After annealing, the perovskite thin films were washed using isopropanol (IPA) to remove the residual CH_3NH_3I on the surface. Details on the fabrication of the perovskite thin films have been described in the literature.

Ellipsometry measurement: Three samples with different layer structures of glass/ITO, glass/ITO/PEDOT:PSS and glass/ITO/PEDOT:PSS/perovskite were prepared. Ellipsometry measurements over the wavelength range of 300 nm-1100 nm in steps of 5 nm were performed in air using *J.A. Woollam V-VASE*. The angles of light incidence were operated between 55˚ and 75˚ relative to the surface normal in steps of 10˚ for reflection ellipsometry and between 40˚ to 60˚ relative to the surface normal in steps of 10˚ for transmission ellipsometry. The depolarisation data were also measured to evaluate the surface roughness. The analysis of the ellipsometric data was performed using the software *WVASE32* (*J. A. Woollam Co.*). The ellipsometric data of the glass/ITO sample was first analysed to obtain the optical constants of the ITO

thin film. The optical constants of ITO were fitted using a Kramers-Kronig consistent model, which consists of a Gaussian oscillator and a Drude model. The thickness and optical constants of ITO were treated as known parameters in the analysis of the glass/ITO/PEDOT:PSS sample. A Tauc-Lorentz oscillator was used to fit the optical constants of PEDOT:PSS. Finally, the extracted optical constants and thicknesses of PEDOT:PSS and ITO were all treated as known parameters in the analysis of the glass/ITO/PEDOT:PSS/perovskite sample. The thickness of the perovskite thin film was determined by assuming that n obeyed the Cauchy equation and that $k = 0$ in the wavelength range of 900-1100 nm (transparent region). With the obtained perovskite layer thickness, n and k were independently varied wavelength-by-wavelength across the entire spectral range to fit the ellipsometric data using the point-by-point method. The extracted wavelength-by-wavelength optical constants were then used as reference values to construct a Kramers-Kronig consistent oscillator model. Five Gaussian oscillators were used in the model to describe the absorption of the perovskite film. The thickness and the oscillator model were then used to directly fit the measured ellipsometric data to further ensure the authenticity of the extracted optical constants and thin-film thickness. Two effective medium approximation (EMA) layers consisting of perovskite and a certain percentage of voids (air) were used to account for the surface roughness of the perovskite thin film. The thicknesses of the perovskite and EMA layers and the percentages of voids in the EMA layers were all set as fitting parameters in the oscillator model to fit the measured ellipsometric data.

Optical simulation: A home-built panchromatic optical field simulation program based on the transfer matrix method was utilised to model the optical field distribution.[43, 55] The program was coded in Matlab™. The light propagation within the range of 360-1200 nm was simulated within all devices structures. The spatial exciton (or electron-hole pair) generation profile was calculated using the following equation:

$$Q_a(x,\lambda) = \frac{1}{2}c\varepsilon_0\alpha_a(\lambda)n_a(\lambda)\left|E_a(x)\right|^2, \tag{1}$$

$$\alpha_a(\lambda) = \frac{4\pi k_a(\lambda)}{\lambda}, \tag{2}$$

where $Q_a(x,\lambda)$ is the photon absorbed and exciton formed at position x in the active layer, c is the speed of light, ε_0 is the permittivity of free space, $n_a(\lambda)$ is the refractive index of the active layer, $E_a(x,\lambda)$ is the electric field at position x in the active layer, $\alpha_a(\lambda)$ is the absorption coefficient, $k_a(\lambda)$ is the extinction coefficient of

the active layer, and λ is the wavelength. The E.Q.E. spectrum of the device was further calculated using the following equation:

$$E.Q.E.(\lambda) = \int \frac{Q_a(x,\lambda)}{\frac{1}{2}c\varepsilon_0 \left|E_0(\lambda)\right|^2} dx, \tag{3}$$

where $E_0(\lambda)$ is the electric field of the incident light in free space. The E.Q.E. calculation assumed that the device possessed 100% internal quantum efficiency (I.Q.E.), *i.e.,* every absorbed photon contributed an electron-hole pair and no carrier recombination occurred during transport. The J_{sc} was calculated by integrating the product of standard AM 1.5G, 1 sun photon flux density and E.Q.E. over the entire wavelength range.
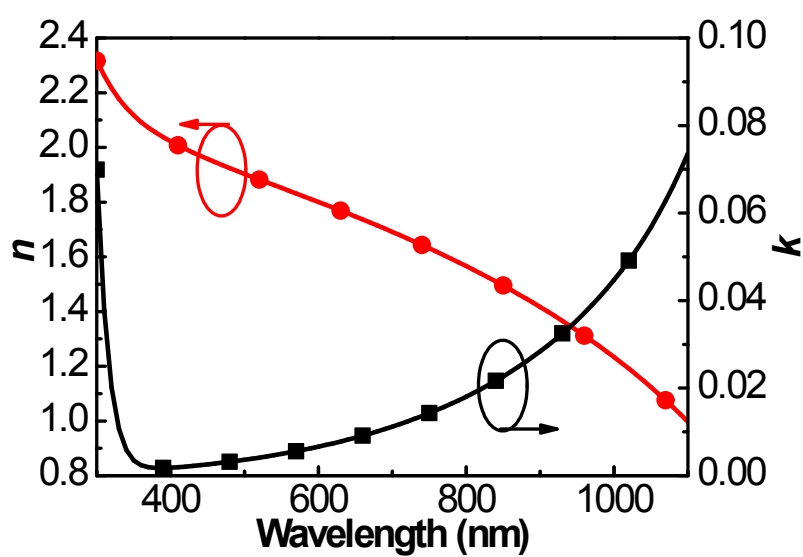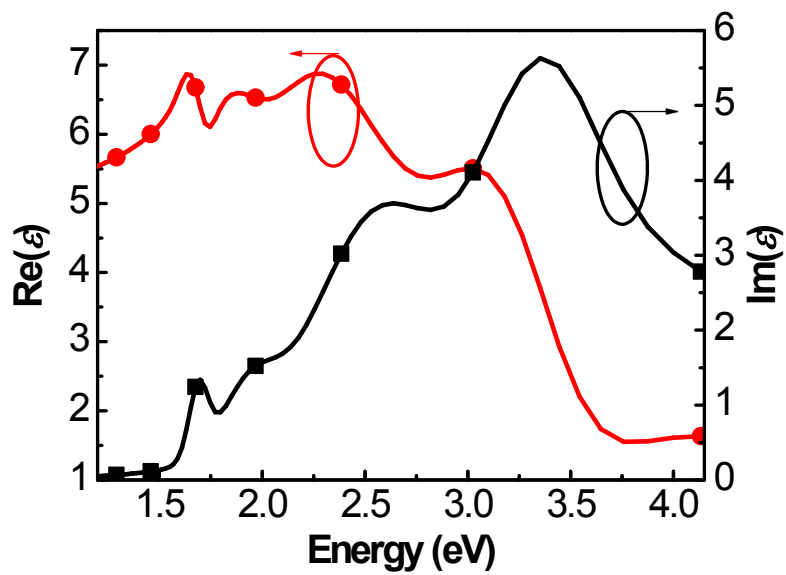
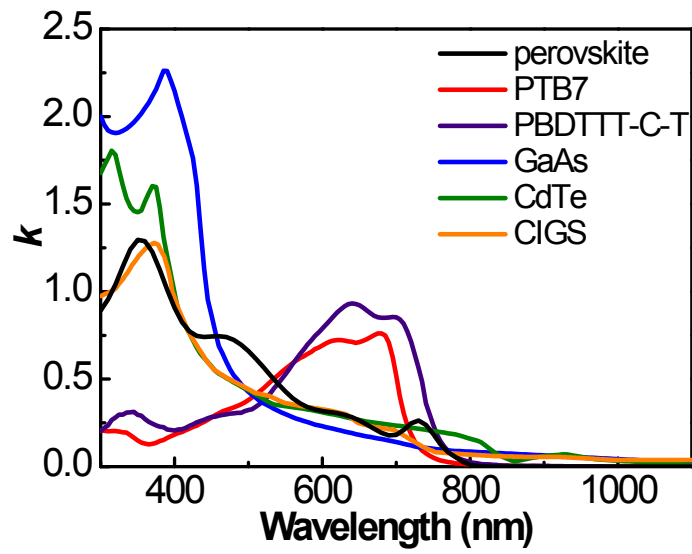**Figure S1.** Refractive index (*n*) and extinction coefficient (*k*) spectrum of ITO.
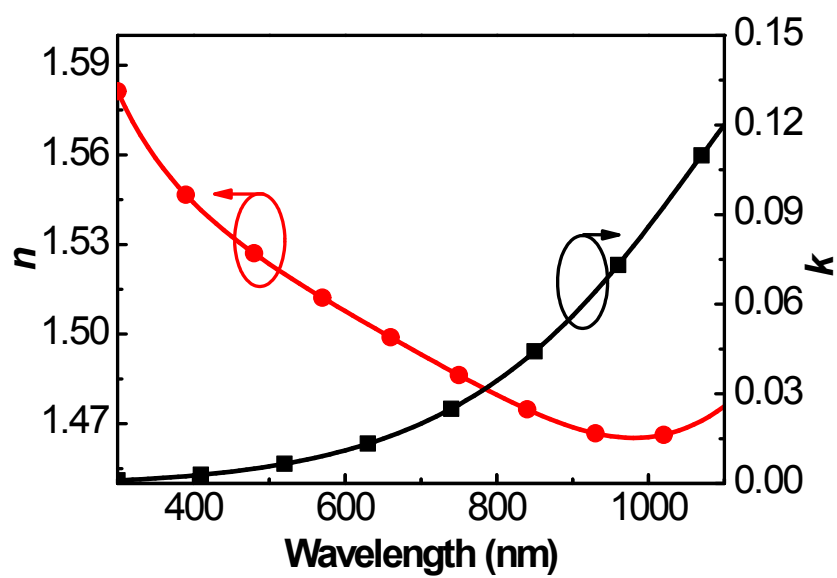
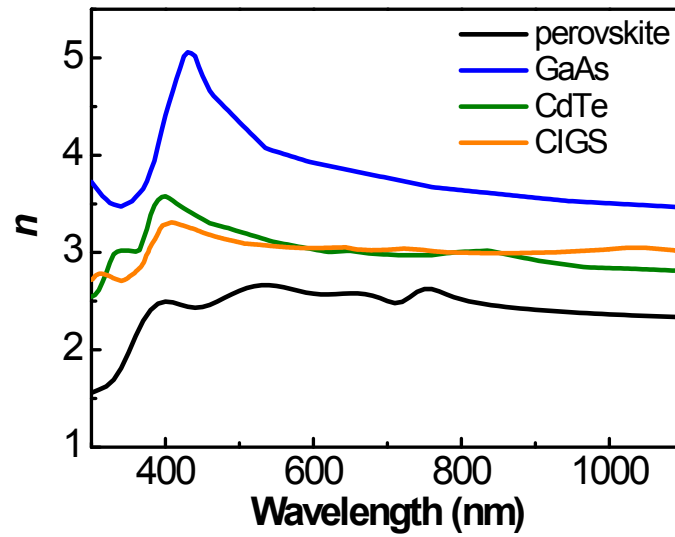**Figure S2.** Refractive index (*n*) and extinction coefficient (*k*) spectrum of PEDOT:PSS.
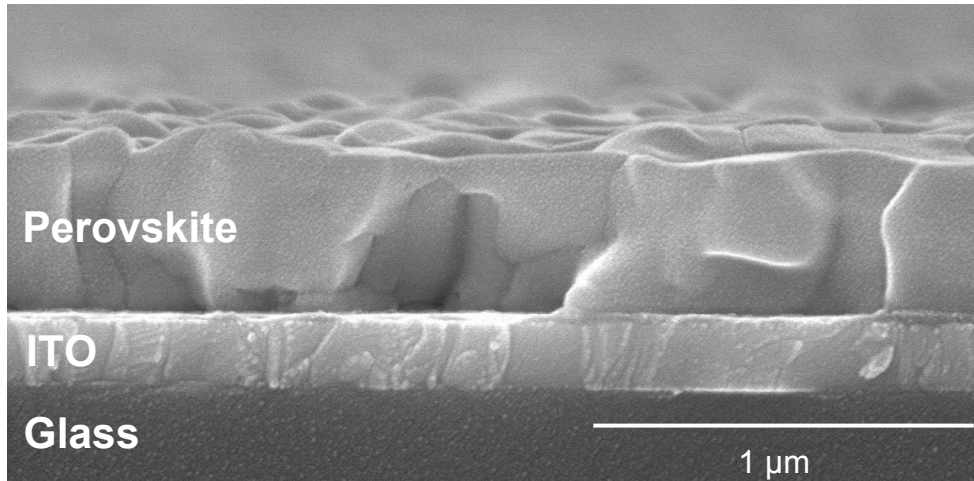
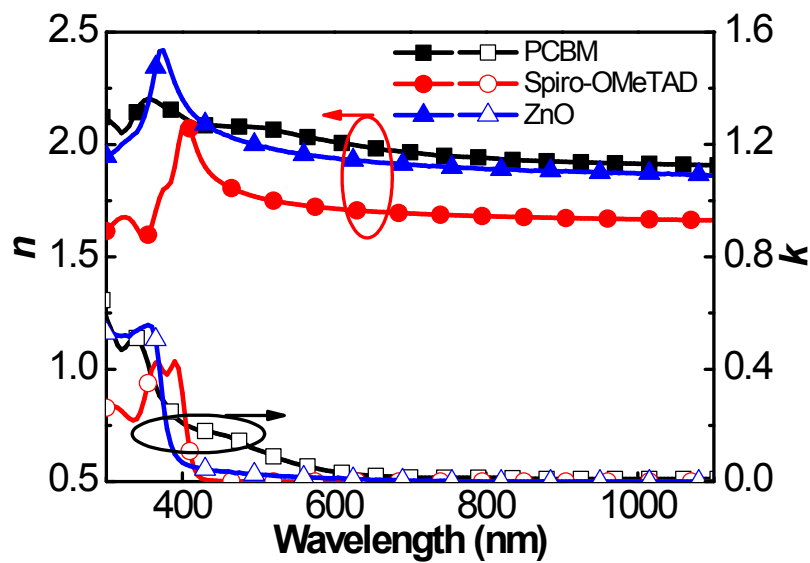**Figure S3.** Cross-sectional SEM image of perovskite thin film on glass/ITO

Figure S4. Real (Re(ε)) and imaginary parts (Im(ε)) of the dielectric constants of CH$_3$NH$_3$PbI$_{(3-x)}$Cl$_x$ thin films.
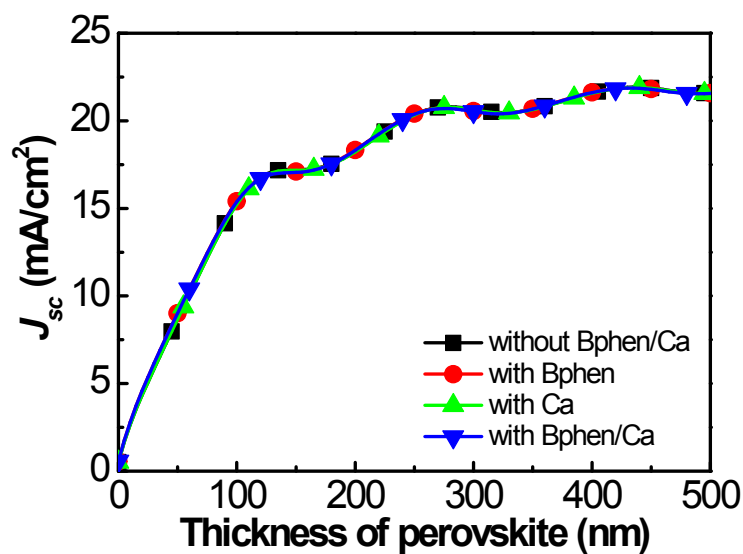
**Figure S5.** Extinction coefficients (k) of $CH_3NH_3PbI_{(3-x)}Cl_x$, PTB7, PBDTTT-C-T, GaAs, CdTe and CIGS thin films.

Figure S6. Refractive indices (n) of $CH_3NH_3PbI_{(3-x)}Cl_x$, GaAs, CdTe and CIGS thin films.

Figure S7. Refractive index (n) (solid) and extinction coefficient (k) (open) spectra of PC$_{60}$BM, Spiro-OMeTAD and ZnO, respectively.


Figure S8. The simulated J_{sc} vs. perovskite layer thickness of normal-type device with and without Bphen and Ca thin films, respectively. Device structure: ITO (140 nm)/PEDOT:PSS (40 nm)/perovskite (0~500 nm)/PC$_{60}$BM (100 nm)/Bphen (0, 6 nm)/Ca (0, 1 nm)/Ag (120 nm).
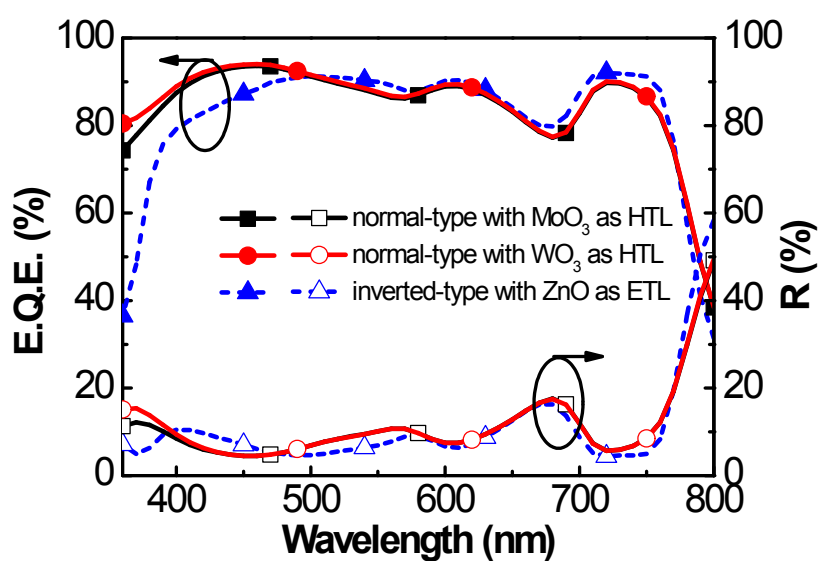
Figure S9. The E.Q.E. and reflectance spectra of the normal-type device with MoO_3 and WO_3 as HTLs and inverted-type device with ZnO as the ETL. The normal-type device structure: ITO (140 nm)/ MoO_3 or WO_3 (20 nm)/perovskite (435 nm)/$PC_{60}BM$ (100 nm)/Ag (120 nm). The inverted-type device structure: ITO (140 nm)/ZnO (40 nm)/perovskite (435 nm)/Spiro-OMeTAD (300 nm)/Ag (120 nm).
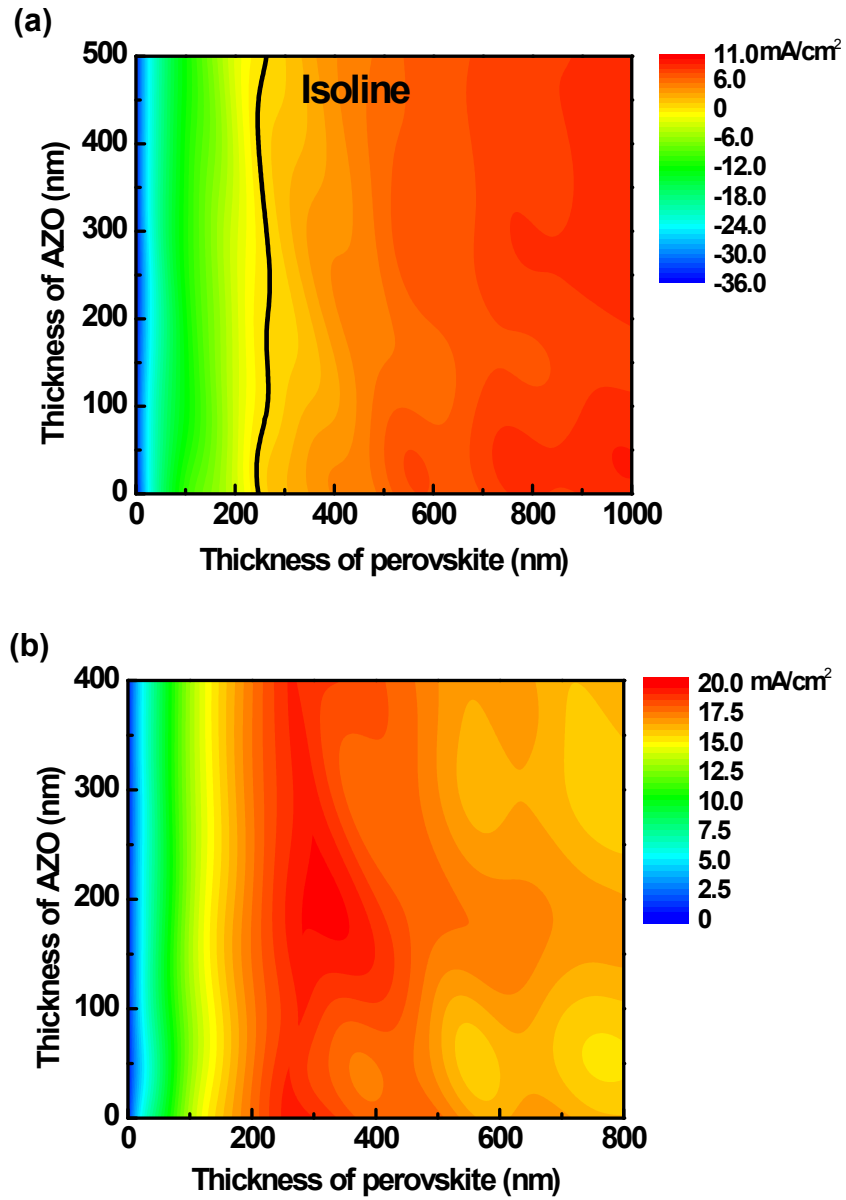
Figure S10. (a) The contour plot of mismatched J_{sc} values. Device structure: AZO (50 nm)/C$_{60}$ (10 nm)/front perovskite layer (0~1000 nm)/MoO$_3$ (5 nm)/AZO (0~500 nm)/ZnO (60 nm)/ZnS (20 nm)/back CIGS layer (2500 nm)/Mo (1000 nm) . (b) The achievable J_{sc} of perovskite/CIGS tandem cell with respect to the AZO and perovskite layer thicknesses.
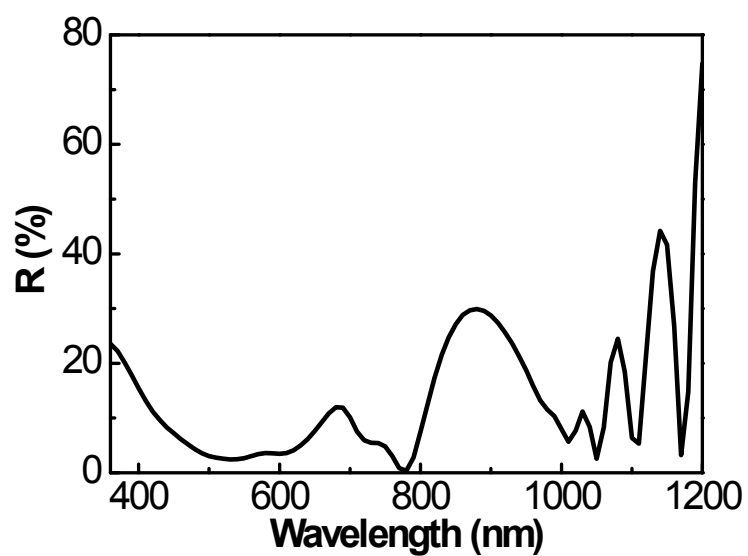
Figure S11. The reflectance spectrum of the optimised perovskite-CIGS tandem device. Device structure: Mo (1000 nm)/CIGS (2500 nm)/ZnS (20 nm)/ZnO (60 nm)/AZO (220 nm)/ MoO_3 (5 nm)/perovskite (270 nm)/C_{60} (10 nm)/AZO (50 nm).